Chapter 12

Symbiosis in Plasmonic Nanoparticles

Abhinav Malasi and Ritesh Sachan

Additional information is available at the end of the chapter

http://dx.doi.org/10.5772/intechopen.71730

Abstract

The focus of this chapter is on how the symbiotic relationship existing in nature can easily be translated to the nanoscale systems, particularly in plasmonic nanoparticles. Here, we discuss the synthesis and properties of bimetallic nanoparticles, consisting of plasmonic silver (Ag) with ferromagnetic cobalt (Co). The symbiotic properties in the Co-Ag bimetallic plasmonic nanoparticles are discussed in the chapter where Ag and Co are the beneficiary elements due to the presence of each other. These bimetallic plasmonic nanomaterials demonstrate multi-functionalities which are not just limited to well-known bio-sensing or magneto-optical effects but also expand to highly unexpected and exotic properties such as extreme oxidation resistance, ferroplasmons, improved quality factor, and tunable radiative quantum efficiency.

Keywords: plasmonics, ferromagnetic, bimetallic nanoparticles, symbiosis, ferroplasmon, quantum efficiency, quality factor, EELS, galvanic coupling, nanosphere lithography, dewetting

1. Introduction

Symbiosis is a natural phenomenon where the co-existence of two entities mutually benefits their survival. Symbiosis is the key ingredient for the existence of life on this planet whether on the surface or under the water. Some of the most common and sought out symbiotic pairs on land are honey bee and flower, birds/mammals and fruit of plants, and in the oceans are corals and algae or clown fish and sea anemones [1]. Even the plants coexist with the natural environment in which the ecosystem and its evolution are symbiotic [2].

This behavior, when observed at the nanoscale, is expected to lead to many interesting phenomena in the field of nanomaterials. For symbiosis to occur at the nanoscale, multi-metallic nanoparticle systems are required where individual components can mutually benefit

and introduce multi-functionalities. In the field of nanomaterials, there is a deliberate drive towards synthesizing materials with multiple functionalities in a single nanostructure and the most simplistic system is bimetallic nanoparticles. The studies on bimetallic nanoparticle systems have shown improved magneto-plasmonic response, enhanced catalytic activities, efficient energy conversion, tunable plasmonic properties, leading to phenomenon like plasmon hybridization and Fano resonances (the interference between narrow bandwidth plasmons and the broader plasmons/continuum) to name a few [3–7]. These properties exhibited by multi-metallic nanomaterial system and has led to the seminal research on the symbiosis in bimetallic particles at the nanoscale. The focus of this book chapter is on the symbiotic properties of bimetallic nanoparticles, particularly those of silver (Ag), an excellent plasmonic material, and cobalt (Co), a ferromagnetic material. These material systems find applications in sensing of biological and chemical agents, catalysis, energy harvesting, data storage, and nanoelectronics.

The contents of the book chapter are organized as follows: Section 2 covers the synthesis techniques involved in the fabrication of bimetallic Co-Ag nanoparticle arrays; Section 3 focuses on the basic characterization techniques that were involved in various studies discussed in Section 4. In Section 4, a detailed discussion on the various symbiotic properties is presented followed by a discussion on other existing symbiotic systems in Section 5 and concluding remarks in Section 6.

2. Synthesis of bimetallic nanoparticles

The synthesis of bimetallic nanoparticles has been reported by both physical and chemical routes using the top-down as well as bottom-up approaches. In the view of this focused chapter, the techniques using physical vapor deposition of metal thin films are specifically emphasized. The two discussed techniques viz. (i) pulsed laser induced dewetting (PLiD) and (ii) colloidal lithography, are adopted due to their merits of being robust, time efficient and comparatively cost efficient as compared to other methods incorporating vapor deposition systems.

2.1. Pulsed laser induced dewetting (PLiD)

The nanoparticles synthesized by PLiD fall in the category of self-organization. Self-organization is a phenomenon in which the intrinsic force plays a prominent role in arranging the patterns with definite length scale and shape, thus stabilizing the system. Some of the common examples of self-organization are skin pigmentation in animals and solar system. At the nanoscale, examples of self-organization can be seen in protein folding self-assembly, the formation of micelles and droplet formation from the breakage of thin polymer and metal films. The phenomenon of breaking of thin metal or polymer films into droplets is called spinodal dewetting which leads to characteristic size and spacing [8–10]. Spinodal dewetting works on the principle of thermodynamic instabilities occurring due to the mismatch in the surface energy of a thin liquid metal film on the non-wetting substrate surface, which leads

to the breakage of the film to more stable state in the form of droplets. Some of the most common examples of spinodal dewetting are the hydrophobic leaf surfaces, oil droplet formation on the water surface, the windshield of vehicles after rain etc. This technique has been used to synthesize a wide variety of nanoparticles of different sizes, shapes, and materials.

The SEM in **Figure 1(a)** shows the typical Co-Ag nanoparticle arrays of dewetted metal film. The inset of the figure depicts the mono-modal size distribution. The average nanoparticle size and spacing of the dewetted nanoparticles depends on the initial film thickness. This gives the control to precisely synthesize the desired size of the nanoparticles. The nanoparticle spacing and size cannot be varied independently and are dependent on each other because of material volume conservation [11, 12]. This suggests that by independently controlling the film thickness of individual metals in a bilayer system, a wide size range can be achieved. Using the theoretical relation between the film thickness and the nanoparticle size, a parameter space of nanoparticle size as a function of Ag volume percentage is plotted for total thickness varying in the range 2–20 nm for Co/Ag/SiO_2 and Ag/Co/SiO_2 regions as shown in **Figure 1(b)**. It is interesting to note here that a wide array of nanoparticles of different sizes and composition can be synthesized using this technique. This technique also gives the flexibility to vary the nanoparticle size by keeping the Ag volume fixed or varying the Ag volume amount by keeping the size fixed.

The drawback of dewetting is the lack of independent control of either of the nanoparticle size or spacing which restricts its use for synthesizing nanoparticles within the interacting regime (interparticle spacing ≤ nanoparticle size). If this barrier could be broken, this technique would be highly useful for making large 2D nanoparticles arrays beneficial for plasmonic

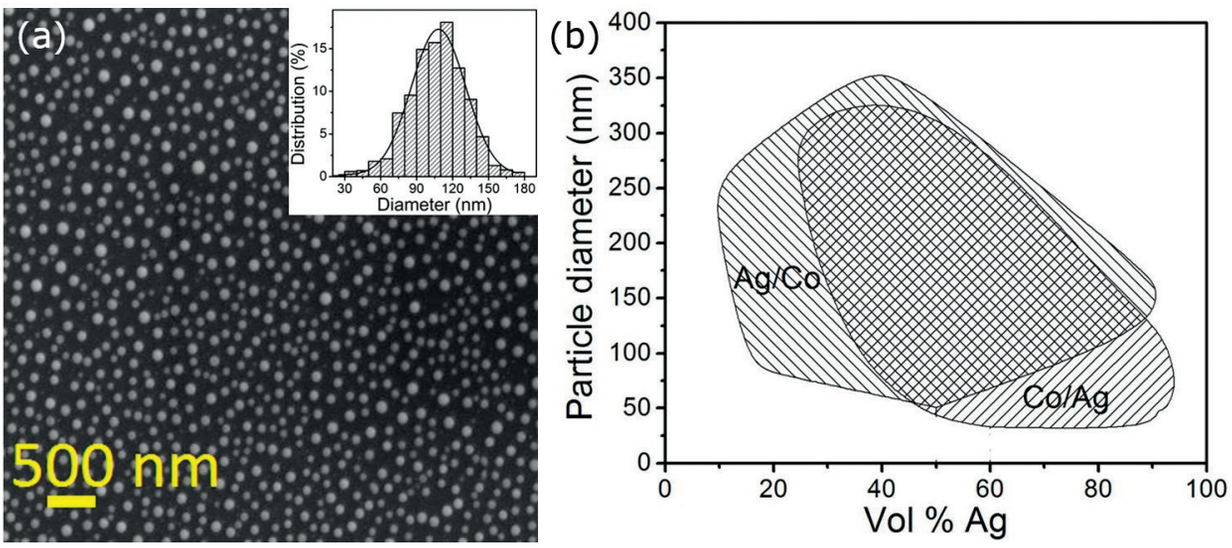

Figure 1. (a) SEM image of Co-Ag nanoparticle with a monomodal size distribution of 113 ± 30 nm. The inset shows the size distribution of the nanoparticles. (b) Theoretically generated nanoparticle size parameter space as a function of Ag amount for the configurations Co/Ag/SiO_2 and Ag/Co/SiO_2 with the total film thickness of the system varied between 2 and 20 nm. (a) from [13] is used in accordance with the Creative Commons Attribution (CC BY) license (https://creativecommons.org/licenses/by/4.0/). (b) is reproduced from Ref. [12]. © IOP Publishing. Reproduced with permission. All rights reserved.

related research requiring energy hotspots. Recently, Yadavali and Kalyanaraman reported that the particle spacing of the nanoparticles can be independent of the initial film thickness which is not the case in classical spinodal dewetting by creating Rayleigh-Taylor instabilities at the metal film surface in contact with liquid creating large pressure gradients due to evaporation [14].

2.2. Colloidal lithography

Lithographic techniques are well suited towards making large area 2D periodic ordered structures. The formation of these periodic structures involves the three basic steps, i.e. mask formation, material deposition, and mask etching. It gives the flexibility to print complex geometries of ordered 2D arrays of nanostructures on large areas. The drawback to most of the lithographic techniques are the cumbersome steps to achieve the final product which is time and resource consuming, and also requiring the use of expensive instruments. Van Duyne and co-workers came out with a fast and inexpensive technique to pattern large area 2D periodic nanostructures by forming masks of self-assembled colloidal nanoparticles called the nanospheres lithography (NSL) [15]. The self-assembly of a monolayer of hexagonally packed colloidal nanoparticles can be either done on hydrophilic substrates or at the air-water interface [15, 16]. Once the mask is ready, the metal is deposited through the gaps between the colloidal beads arrangement. The template is then etched, leaving the hexagonally arranged patterns of metal nano-triangles on the substrate. The in-plane dimensions of the features formed by NSL depend solely on the size of the colloidal nanoparticles [15].

The biggest challenge using this technique is to avoid the formation of a large number of vacancy and dislocation defects [17]. To tackle the control of defect formation is to control the evaporation rate of the fluid containing the beads [18, 19]. The evaporating fluid forces the beads to move towards the crystallized area due to the internal flow of the fluid. Other ways are to confine the solution and apply mechanical or physical force by gas flow to form ordered arrangement [16, 20, 21].

NSL requires the direction of metal flux being deposited to be perpendicular to the substrate plane. This restricts the control to vary the nanoparticle geometry and is limited to nano-triangles, which are truncated pyramids and can be further tuned to semi-spherical shape [22, 23]. Many variations of colloidal lithography in the form of angle-resolved NSL, shadow-sphere lithography, hole mask colloidal lithography, and shrinkable hole mask lithography exists which can create complex geometries like crescents, dimers, pillars, chiral structures etc. [24–27].

3. Characterization

The as-prepared samples were characterized for their morphology by SEM and optical properties by UV-vis spectroscopy. The statistical information on the average nanoparticle size and distribution were calculated by analyzing the SEM images using image analysis software (ImageJ by NIH) [28]. EDX mapping study on bimetallic Co-Ag nanoparticles revealed the

http://dx.doi.org/10.5772/intechopen.71730

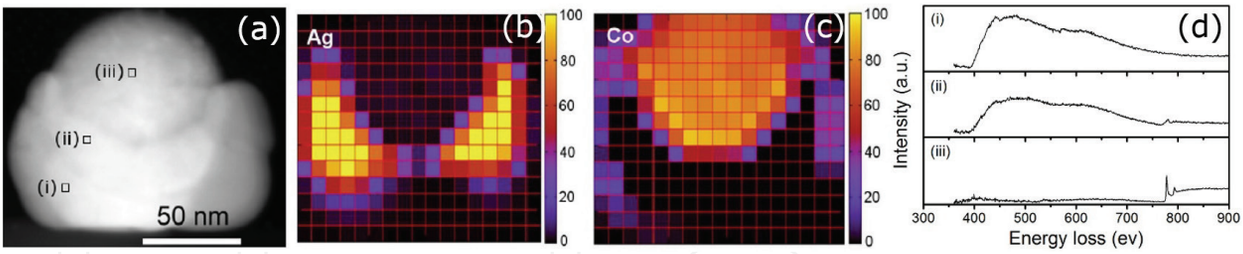

Figure 2. (a) Cross-sectional HAADF image of Ag-Co hemispherical nanoparticle synthesized by PLiD. Core-loss EELS mapping of (b) Ag and (c) Co for the hemispherical nanoparticle. (d) The EELS spectra measured for the nanoparticle measured at three different regions marked in (a). Reproduced from Ref. [12]. © IOP Publishing. Reproduced with permission. All rights reserved.

volume ratio of the two metals remained intact after the nanoparticle synthesis. EDX analysis revealed the average Co:Ag X-ray count of the synthesized nanoparticles followed a linear relationship with the Co:Ag film thickness ratio [12].

In the present case of characterizing symbiotic bimetallic nanoscale systems, core-loss EELS (electron energy loss spectroscopy) is employed to understand the elemental distribution, inter-mixing or alloying, chemical reactivity and electronic structure in a single nanoparticle. An example is shown in **Figure 2** where the elemental distribution of Ag and Co is mapped using Ag-M_{45} and Co-L_{23} edges in bimetallic nanoparticles. A high-angle annular dark field (HAADF) image of Ag-Co bimetallic nanoparticle is shown in **Figure 2(a)**, along with the Ag (**Figure 2(b)**) and Co (**Figure 2(c)**) elemental maps. The representative core-loss EELS edges of Ag and Co obtained from the region (i), (ii) and (iii) regions are shown in **Figure 2(d)** [12]. This method is also used to quantify the surface oxidation in the Ag-Co nanoparticles and to study the oxidation state of formed metal oxides [29]. The information about the optical behavior is also obtained using low-loss EELS and will be discussed in Section 4.3.

4. Symbiotic properties

In this section, we discuss the tuning and improvement or enhancement in four different properties caused by the mutual sharing or transfer of free electrons between Ag and Co, leading to symbiosis at the nanoscale.

4.1. Tuning the plasmon resonance and its sensitivity

The materials displaying optical properties at the nanoscale are termed as plasmonic materials. Plasmonics can be defined as when the metal nanoparticles interact with light of sizes less than or equivalent to the wavelength, the free electrons start to resonate at a certain frequency called the plasmon resonance frequency. The plasmon resonance is a material property and depends on the shape, size, composition, and environment of the nanoparticle. The other viable option to vary the plasmon resonance is by synthesizing multi-metallic nanoparticle composites. Multi-metallic nanoparticles open the door to incorporate multiple functionalities in a single nanoparticle. Depending on the synthesis approach and the reaction conditions,

amount of mixing of metals within a nanoparticle can vary from being immiscible like core-shell, to partially miscible, or to completely miscible and also gives advantage on tuning the nanoparticle morphology from spheres to rods and from discs to crescents [30, 31].

Kalyanaraman and co-workers extensively studied the Ag-Co bimetallic system synthesized by PLiD [11, 12, 29, 32–35]. Two separate studies were conducted on these bimetallic nanoparticles, one in which the bimetal composition was fixed while the nanoparticle size was varied. In the other case, the Ag amount was fixed and the Co amount was varied. In the first study, three different compositions of Ag (71.5%, 83.3%, and 100%) in the nanoparticles were studied which were achieved by keeping the starting volume ratio of the metals fixed. It was observed that for fixed composition and increasing nanoparticle size, the plasmon resonance red shifted as shown in **Figure 3(a)**. This observation is explained by using Maxwell-Garnett (MG) approach. The MG approach calculates the effective complex dielectric of a system in which small grains of metal 1 are embedded in metal 2, and is only dependent on the volume fraction and complex dielectric functions of the metals, suggesting for fixed composition, the effective complex dielectric should be the same [36]. Hence an increase in size shifts the plasmon to higher wavelength, consistent with the plasmonic theory. For the

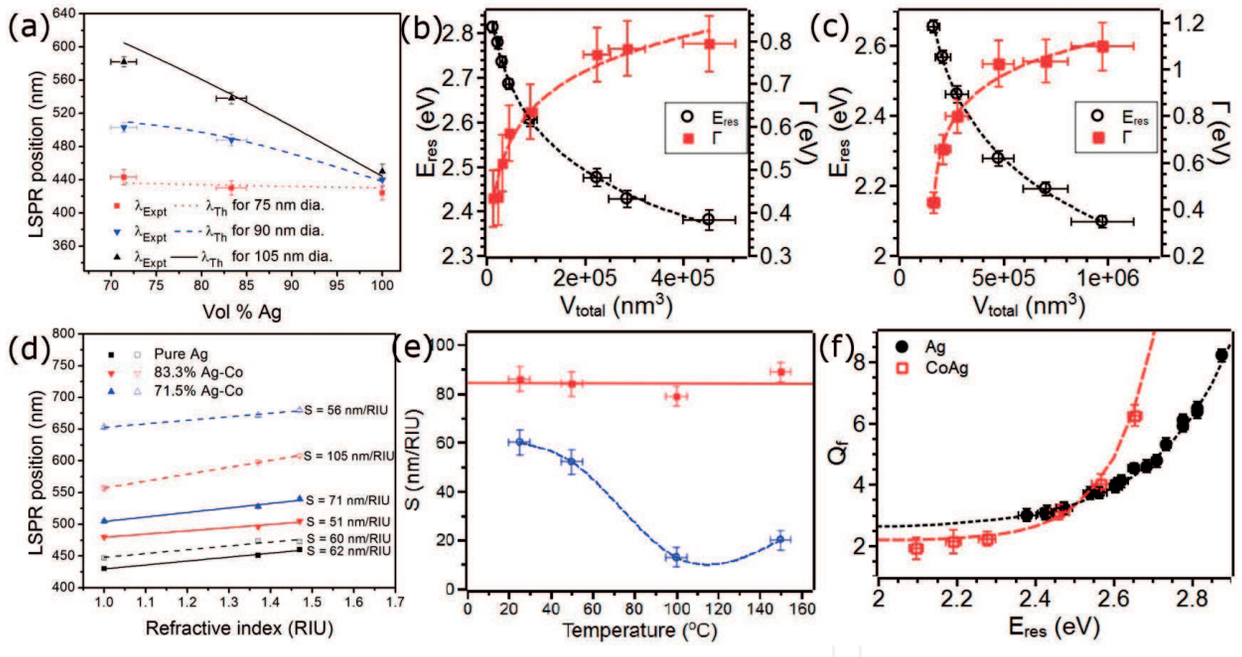

Figure 3. (a) Comparison of the localized surface plasmon resonance (LSPR) wavelength for different composition of Ag in a single nanoparticle as a function of three different nanoparticle sizes. (b) and (c) Comparison of the plasmon resonance energy and bandwidth of pure Ag and Co-Ag nanoparticles as a function of total nanoparticle volume, respectively. (d) LSPR positions of three different compositions of Ag measured at three different refractive index liquids. The slopes of the straight-line fits give the refractive index sensitivity of the nanoparticles denoted by *S*. (e) Refractive index sensitivity comparison of Co-Ag and Ag nanoparticles synthesized from 1 nm Co on 5 nm Ag and 5 nm Ag as a function of annealing temperature (modified color scheme). (f) Experimentally measured quality factor comparison of different compositions of Co-Ag nanoparticles and different sizes of Ag nanoparticles as a function of their plasmon resonance energy. (a) and (d) from Ref. [12]. (b), (c) and (f) from Ref. [13], (e) reproduced with permission from Ref. [29].

second study, nanoparticles were synthesized by dewetting of stacked Co/Ag/SiO_2 system. The optical properties of different sized nanoparticles were studied by varying the thickness of Co film from 1 to 5 nm while keeping the thickness of Ag film fixed at 5 nm. Similarly, pure Ag nanoparticles were synthesized by varying the initial film thickness from 1 to 10 nm. The plasmon resonance energy and plasmon bandwidth for Ag and Co-Ag nanoparticles as a function of nanoparticle volume are plotted in **Figure 3(b)** and **(c)**, respectively. Similarly, on increasing the nanoparticle volume, the plasmon resonance energy decreases or red-shifts and the nanoparticle bandwidth increases.

After tuning the plasmon resonance energy, the sensitivity and stability of these nanoparticles are tested. On conducting the refractive index (RI) sensing of the bimetallic nanoparticles, it is observed that for some composition and sizes of Co-Ag nanoparticles, they showed improved RI sensitivity over pure Ag nanoparticles, shown in **Figure 3(d)**. In another study, bimetals of Co-Ag nanoparticles (83.3% Ag) heated to 150°C, showed stable RI sensitivity while Ag nanoparticles for the same starting film thickness are highly unstable as evident from **Figure 3(e)**. The reason for this ultra-stability is discussed in Section 4.2. A general idea about the sensor's performance can also be acquired by calculating its quality factor. The quality factor is a direct measure of the sensitivity of a system to detect, higher the quality factor means more sensitive the system. For a plasmonic sensor, the experimental quality factor can be calculated as $Q = E_{res}/\Gamma$, E_{res} being the plasmon resonance energy and Γ the bandwidth of the plasmon resonance. The quality factor comparison of the samples discussed in second study is plotted as a function of resonance energy in **Figure 3(f)**. The crossover of the quality factor in **Figure 3(f)** is explained by comparing the bandwidths (**Figure 3(b)** and **(c)**) of the two systems for plasmon resonance energies greater than 2.5 eV. At the same plasmon resonance energy, the nanoparticle with higher quality factor means that it has a narrow bandwidth. This leads to the question: what are the different factors contributing to the broadening of plasmon bandwidth?

To explain the broadening of the bandwidth, we use the two-level model to explain the results, which is analogous to molecular spectroscopy in which the plasmon decays by dephasing of coherent oscillations (remember the definition of plasmon, which is a coherent oscillation of electrons) [37]. The dephasing occurs as a result of many interactions occurring due to electron-electron, electron-phonon, electron-defect and electron-surface interactions [37, 38]. These events follow Matthiessen's rule as these scattering events are statistically independent channels and thus can be added up [37, 38]. So, the total bandwidth of Co-Ag bimetallic nanoparticles should be the sum of the contributions from individual metals, which clearly is not the case as seen in **Figure 3(f)**. This leads to the possibility of some sort of electronic interaction taking place at the nanoscale between Ag and Co. It also suggests that the sensitivity is highly dependent on nanoparticle size and composition, as evident from **Figure 3(d)**.

4.2. Oxidation stability

Metal structures at the nanoscale have high reactivity and so are susceptible to oxidation. Because of this reason, Ag which has the best optical properties is not favored over Au [39]. The inertness of Au makes it a more plausible material than Ag which scums to its chemical

and structural instabilities [40, 41]. Shortage of stable plasmonic materials creates the demand for research on alternate or new stable plasmonic materials required for various applications at the nanoscale [42, 43]. A lot of different solutions or alternative routes have been presented to stabilize metal nanoparticles but they either are short-term solutions or undermine the pure metal properties. The brighter side of these solutions has resulted in finding new and improved properties in some cases. By synthesizing core-shell of Au-Ag, the Ag could be stabilized via electron transfer from Au core, but the nanoparticle properties degrade over time due to the alloying between Au and Ag at the interface [44]. These synthesized core-shell structures at a critical thickness of Ag shell are resilient to harsh chloride ion environment without any visible degradation under transmission electron microscope.

In another study, the Ag nanostructures were stabilized by processing them with low-temperature single hydrogen atoms. The idea was to stabilize nanostructures by filling the interstitial sites with a hydrogen atom to prevent Ag atom diffusion [41]. Covering Ag nanostructures with a monolayer of graphene could protect them from oxidation for almost a period of a month [45]. The other possibility is by surface passivation of Ag nanostructures with organic molecules. The choice of an organic molecule can preferentially control the optical or the electrical properties [46].

Sachan et al. stabilized the Ag nanoparticles by synthesizing bimetals of Ag and Co having segregated regions within a single nanoparticle using PLiD. The oxidation behavior was studied using optical spectroscopy and core-loss EELS mapping and showed prolong optical stability of Ag nanoparticles [12, 29, 34]. This ultra-stability was due to the galvanic coupling between Co and Ag at the nanoscale where Co was acting as a sacrificial anode, thus protecting Ag surface by providing electrons as shown in **Figure 4(a)**. The study was further extended by Malasi et al. to understand the role of Co composition in these bimetals and how the Co-Ag nanoparticle life could be extended [34]. On studying the extended optical bandwidth decay of these nanoparticles, two observations were made. Firstly, the decay behavior of Co and Ag of the bimetals followed two different trends displaying a sharp boundary demarcating the change in trends from inverse logarithmic to exponential decay shown in **Figure 4(b)**. Second observation suggested that the decay trends observed in pure metal oxidation were consistent with the decay of the individual metals of the bimetallic nanoparticle and overlapped perfectly. The change in decay behavior suggested that the two metals have segregated regions, the results of which are consistent with the EELS observation. The only question that remained here to answer was whether the Co oxidized completely or not before the change in the optical bandwidth decay trends. To answer this, a theoretical model is used to quantify the oxidation of Co in the bimetallic nanoparticle system, details of which are available in Ref. [34]. Co-Ag bimetals showed almost 12 times better shelf life than pure Ag nanoparticles for 50% degradation in the optical bandwidth and depending on Co amount, the Ag could be oxide free for almost a year. The lifetimes were established using effective medium theory, which is a versatile way to study nanoparticles in embedded media [47, 48].

To explore the other possibilities of stability studies in Co-Ag bimetal system, Kalyanaraman and co-workers studied the extraordinary optical transmission (EOT) of perforated holes of triangular shapes in Ag and Ag/Co films [49]. The findings suggested that Ag films deposited

http://dx.doi.org/10.5772/intechopen.71730

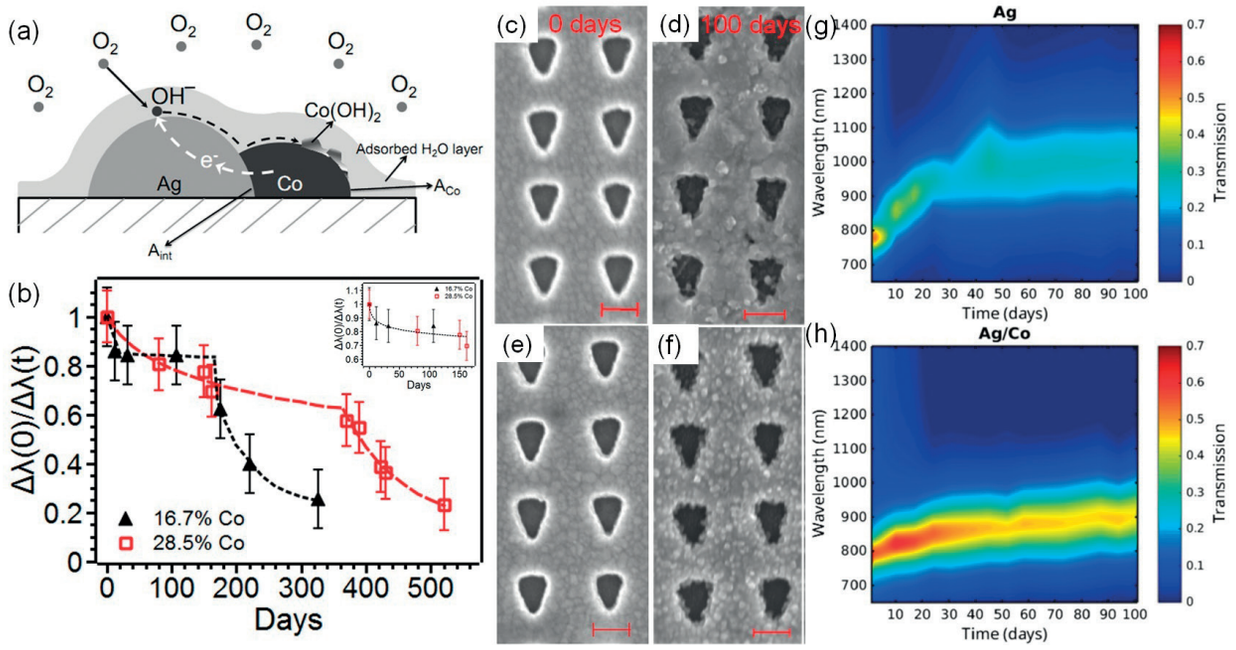

Figure 4. (a) Schematic showing the galvanic coupling in a single bimetallic Co-Ag nanoparticle. (b) Optical bandwidth decay of two different concentrations of Co (solid triangles and hollow squares) in the bimetallic Co-Ag nanoparticles plotted as a function of days. Each curve follows two different trends, inverse logarithmic and exponential decay corresponding to that of pure Co and pure Ag, respectively. The inset shows the overlap of Co oxidation in Co-Ag nanoparticles, where the dashed line is an inverse logarithmic function as a guide to the eye. SEM images depicting the morphology of triangular shaped EOTs of pure Ag captured on (c) 0 days and (d) after 100 days. Similarly, SEM images for the morphology of Ag/Co EOT captured on (e) day 0 and (f) after 100 days. (g) and (h) are the contour maps for the resonance decay of Ag and Ag/Co EOT devices, respectively. (a) reproduced with permission from Ref. [29]. (b) reproduced from Ref. [34]. © IOP Publishing. Reproduced with permission. All rights reserved. (c)–(h) from Ref. [49], used in accordance with the Creative Commons Attribution (CC BY) license (https://creativecommons.org/licenses/by/4.0/).

on top of Co films showed much improved EOT stability in ambient air as can be visualized from the SEM images shown in **Figure 4(c)–(f)**. The study was carried out for 100 days which showed 1.9 times better plasmon peak stability and 1.7 times better bandwidth stability over pure Ag EOT. The contour maps in **Figure 4(g)** and **(h)** shows the plasmon resonance decay as a function of days. The map shows the change in the behavior of Ag EOT, initially the plasmon significantly red-shifts leading up to day 40 after that the plasmon resonance intensity starts decaying very rapidly in comparison to Ag/Co EOT showing slower red-shift and stable plasmon resonance intensity. The stabilization of bimetal EOT is attributed to the underlying Co layer, which prevents Ag to dewet on the glass substrate. This is evident from the SEM images where material build-up is present for pure Ag EOTs due to dewetting on glass substrate but absent in Ag/Co EOTs.

4.3. Ferro-plasmons

As discussed in the preceding sections, due to the scarcity of plasmonic materials or rather stable plasmonic materials at room temperature, a lot of attention has been diverted on the study of bimetallic nanoparticle systems. The interaction between the bimetallic nanoparticles

has led to interesting optical phenomena such as plasmon hybridization and Fano interference resonance. These optical phenomena occur due to the interactions between various plasmon modes, dark and bright modes, or sub-radiant and super-radiant modes. Hybridization of two plasmonic resonances leads to a lower energy resonance, i.e. the sub-radiant mode with narrow bandwidth and the higher energy resonance acting as a continuum, i.e. the super-radiant mode, in asymmetric nanoparticle systems [50, 51]. The above mentioned optical phenomena are observed in a wide variety of plasmonic nanostructures such as multi-shells, cavities, and heterodimers [52–54].

One such optical phenomenon observed in the bimetallic Ag-CoFe and Ag-Co nanoparticles is the ferroplasmon (FP), intense LSPR (localized surface plasmon resonance) excited in the visible spectrum of light on the surface of ferromagnetic CoFe and Co when in contact with plasmonic Ag [32]. FP is an intense LSPR with long plasmon decay length scales in the visible spectrum of light. As mentioned earlier, the exhibition of a strong LSPR in the visible spectrum is the characteristic property of the noble metals (Ag, Au, and Cu). Other metals, including the ferromagnetic metals (e.g. Co, Ni, Fe) have non-existent or highly damped visible plasmons. Recent studies of Ni nanostructures have demonstrated the sustenance of surface plasmon in the visible spectrum of light [55]. The discovery of FP is possible due to the advances in transmission electron microscopy equipped with a monochromated electron probe in STEM with energy resolutions of ~150 meV, enabling the quantitative study of well-resolved plasmon peaks at the nanoscale using low-loss EELS with high energy and spatial resolution. **Figure 5** shows the comparative study of plasmon excitations on the surface of bimetal Ag-CoFe, pure Ag and pure CoFe nanoparticles, resolved by low-loss EELS. The EELS spectra are shown in **Figure 5(a)** from Ag region of Ag-CoFe nanoparticle and the isolated Ag nanoparticle, taken from the square area marked in the HAADF images in **Figure 5(b)** and **(c)**. Both the spectra exhibit peaks in the visible range corresponding to the well-known surface plasmon in Ag. In contrast, the EELS spectrum shown in **Figure 5(e)** obtained from CoFe in Ag-CoFe show a strong and distinct plasmon peak, referred to as FP, at 2.7 eV, unlike the featureless spectrum for the isolated CoFe nanoparticle. The EELS spectra for CoFe corresponds to the red square marked on the CoFe side of the bimetal nanoparticle and the isolated nanoparticle marked on the HAADF images in **Figure 5(b)** and **(d)**, respectively. The evolution of FP in the Ag-CoFe bimetallic system is thoroughly studied as a function of nanoparticle size and found to be consistently present [32]. The presence of FP is an intricate play between the nanoparticle morphology and the interface shared between them, which was demonstrated by the absence of FP in dimers of Ag-Co nano-triangles placed in close proximity [56].

The physical origin of FP is explained by qualitative theoretical models such as dipole-dipole interaction, hybridization model, and Fano interference as these all arise due to the coupling between different plasmon modes [50, 51, 57]. A simple dipole-dipole interaction approach considers the coupling between same (dipole-dipole) or different (dipole-quadrupole) modes and successfully describes the electromagnetic energy transfer between two nanoparticles. However, it lacks the complete explanation due to inherently neglecting the interaction of other modes of plasmon oscillation. Alternatively, another model based on the plasmon hybridization effectively explain the existence of FP peak evolved at 2.7 eV, but also predict

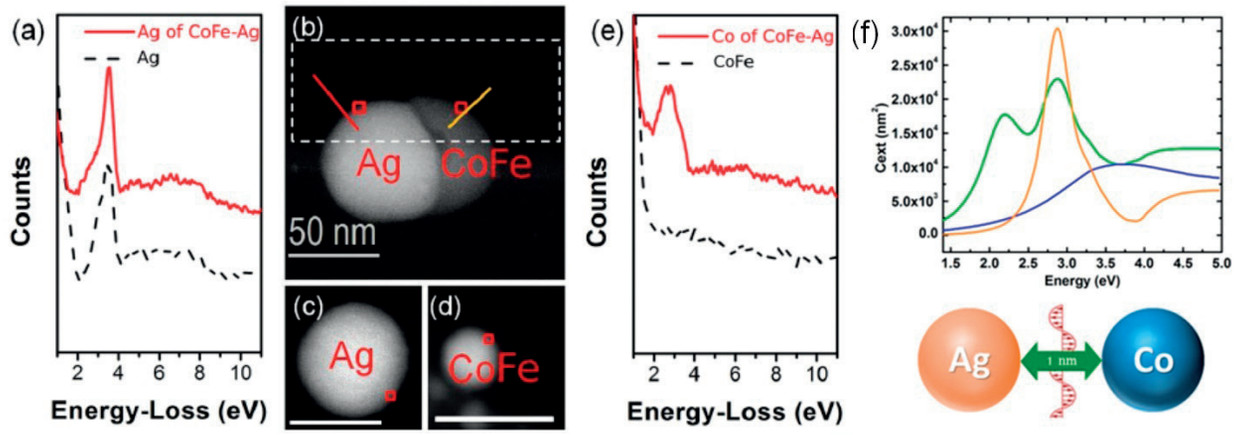

Figure 5. (a) EELS spectra from the surface of Ag side of Ag-CoFe (solid line) and isolated Ag nanoparticle. (b), (c) and (d) are the HAADF images of bimetallic Ag-CoFe, isolated Ag, and isolated CoFe nanoparticles, respectively. (e) EELS spectra from the surface of CoFe side of Ag-CoFe (solid line) and isolated CoFe nanoparticle. The EELS spectra are measured from the small red boxes marked on the HAADF images. (f) Comparison of extinction spectra simulated for pure Ag (orange line), pure Co (blue line) and dimer of Ag-Co (green line) nano-spheres. The schematic represents the Ag-Co dimer system separated by 1 nm. Reprinted (adapted) with permission from [32, 58]. Copyright (2014) American Chemical Society.

additional high-order peak, which is not observed experimentally in EELS. In the hybridization model, the coupling can be assumed as an instantaneous Coulomb interaction between the surface charge density of various components. In another approach, electrodynamic simulations were performed showing the interaction between spherical Ag and Co nanoparticles with their surfaces separated by a nanometer gap [58]. This gives rise to new plasmon mode at higher energy due to the interaction between Ag and Co nanospheres, as shown in **Figure 5(f)** where the optical spectrum of pure Co and pure Ag nanospheres are plotted in blue and orange, respectively. The green color corresponds to the spectrum obtained from the interaction between the Ag-Co nanospheres shown in the schematic. This analytical approach depends on the interaction of two spherical nanoparticles and the use of non-contacting geometry, assuming the contact between Ag and Co will not influence the interaction process. FP nanoparticle system still lacks a detailed theoretical study which is only possible by finite difference time domain or discrete dipole approximation simulations by taking account the hemispherical shaped nanoparticle.

4.4. Radiative quantum efficiency

Plasmonic nanoparticles are an efficient medium for transferring the coupled electromagnetic waves in and out of the system. How well the nanoparticles will couple to the electromagnetic waves depends on their shape, size, material, and ambient dielectric environment and is measured by the radiative quantum efficiency. The dependence of radiative quantum efficiency on the Au nanoparticle shape and size was first demonstrated by Sonnichsen et al. [59]. As the volume of nanostructure increased, the radiative contributions in the bandwidth increased, leading to increased quantum efficiencies. The other interesting observation regarding Co-Ag bimetal system is the tuning of radiative quantum efficiency in a much wider energy range by controlling the Co amount and keeping the Ag volume fixed [13]. This is achieved by

experimentally calculating the radiative and non-radiative contributions in the bandwidth, which are then used to calculate the radiative quantum efficiency calculated as: $\eta = \frac{\Gamma_{1,R}}{\Gamma_{1,R} + \Gamma_{1,NR}}$, where Γ is the bandwidth and subscripts *R* and *NR* stand for radiative and non-radiative respectively.

Continuing the discussion in Section 4.1 on bandwidth broadening, another assumption to consider is to neglect the contributions from electron scattering on the broadening of the bandwidth as discussed in Ref. [13]. The only contributions worth mentioning are the radiative losses and non-radiative absorption. As mentioned earlier, the bandwidth depends on the nanoparticle volume and dielectric function, hence the simplified expression can be written as, $\Gamma_2^{exp}(E_{res}, V) = \frac{1}{2}\Gamma_{1,R}(E_{res}, V) + \frac{1}{2}\Gamma_{1,NR}(E_{res}, V)$, here E_{res} is the plasmon resonance energy and *V* is the nanoparticle volume. Since, Γ_2^{exp} is experimentally measured, and if either one of the radiative or non-radiative contributions could be measured independently, this will lead to calculating the radiative quantum efficiency.

Working under the limit of dipolar approximation, the radiative losses at the plasmon resonance energy are only dependent on the nanoparticle volume and thus can be written as $\Gamma_{1,R}(E_{res}, V) \propto V$ [60]. The proportionality constant *K* is a material parameter of metal understudy and is independent of the nanoparticle volume, shape, size and the dielectric environment. To work under the dipolar approximation, the nanoparticle should follow $V/\lambda^3 \ll 1$, where λ is the wavelength of light. Under this condition, the nanoparticle polarizability is dominated by the dipolar components and higher order multipoles can be ignored. The samples under study followed this approximation and for the size and resonance energy range followed the above condition ($V/\lambda^3 \leq 10^{-2}$). Once it is established that we are working under the dipolar approximation, the proportionality constant *K* is calculated by taking two different geometries having the same plasmon resonance energy as described in Ref. [59]. For our study, we synthesized Ag nano-triangles by NSL technique and used the data of Ag hemispherical nanoparticles to calculate *K*. As, we are working on Ag and at the same plasmon resonance energy, the non-radiative losses (radiative contributions are due to the dielectric of the material) of the two shapes will cancel out. Hence, *K* is calculated, $K = \frac{\Delta\Gamma_{1,R}}{\Delta V} = 2\frac{\Delta\Gamma_2^{exp}}{\Delta V}$. **Figure 6(a)** compares the bandwidth of Ag nano-triangles and hemispheres as a function of plasmon resonance energy. Inset of **Figure 6(a)** shows *K* as a function of plasmon resonance energy with the average $K = 8.1 \pm 2.3 \times 10^{-7}$ eV/nm^3 plotted as a dashed line. The value of *K* is further used to calculate the contributions of radiative and non-radiative components and finally the radiative quantum efficiency.

After establishing the contributions of the radiative and non-radiative components to the broadening of Ag nanoparticle (**Figure 6(b)**), a similar analysis was done for Co-Ag nanoparticles. Consider the two previously established facts: (i) Ag and Co have segregated regions within a single nanoparticle and the average nanoparticle spacing is much greater than the average diameter, hence near-field coupling is non-existent for this case; and (ii) the bimetallic nanoparticle does not follow the Matthiessen's rule as evident from the quality factor calculations discussed previously. So, we proposed the possibility of the modification of the radiative bandwidth of Ag due to the presence of Co. This assumption is made based on the ferroplasmon discovery, since the segregated Ag and Co had plasmons at almost the same resonance

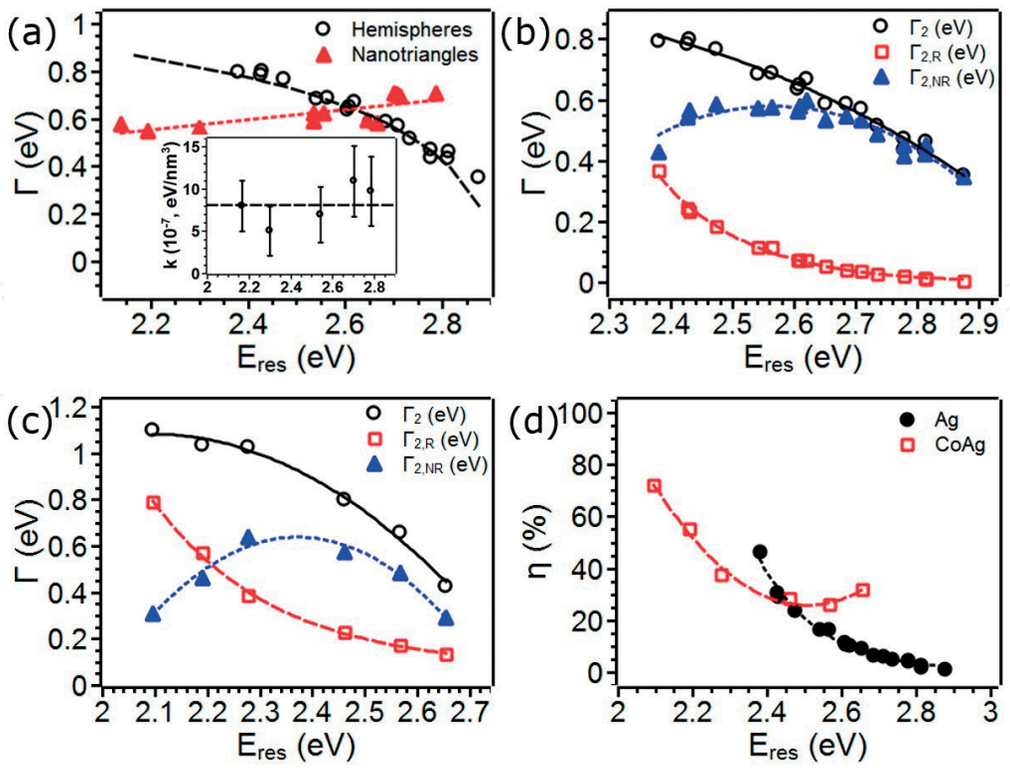

Figure 6. (a) Compares the bandwidth of hemispherical Ag nanoparticles with Ag nano-triangles plotted against plasmon resonance energy. The inset depicts the *K* values calculated at different plasmon resonance energy with the dashed horizontal line depicting the average *K* value. (b) and (c) Plots the total bandwidth with its radiative and non-radiative components against plasmon resonance energy for Ag and Co-Ag nanoparticles, respectively. (d) Radiative quantum efficiency comparison for Ag and Co-Ag nanoparticles as a function of plasmon resonance energy. Ref. [13] is used in accordance with the Creative Commons Attribution (CC BY) license (https://creativecommons.org/licenses/by/4.0/).

energy, further encouraging to assume Co-Ag nanoparticle equivalent to one big Ag nanoparticle of similar volume. Keeping this assumption, we calculated the bandwidth contributions for the bimetallic nanoparticle as previously discussed. The radiative, non-radiative and total experimental bandwidth values for different Co-Ag nanoparticles is plotted as a function of plasmon resonance energy in **Figure 6(c)**.

To support the above assumption, we used an analytical model describing the interaction between two non-bianisotropic systems placed adjacent to each other and within the interaction regime [61]. This metamaterial system of a good (Ag in our case) and poor (Co in our case) conductor is analogous to RLC circuit. The active power of the individual components and the RLC system is calculated to explain the results. It is demonstrated that by increasing the surface to volume ratio, the active power changes sign from negative to positive for Co. An opposite change is observed in the active power for Ag, in the same frequency interval. The cross-over from positive to negative is also observed for the total active power of the system [13]. When surface to volume ratio is small (weak coupling), the total active power remains positive, but as the surface to volume ratio increases, the power switches sign in the frequency interval of study. For the total active power to be zero at a certain frequency, if the active power of Co is zero, then the active power of Ag will also be zero. This suggests that

the presence of Co modifies the power of Ag, which is also our experimental observation. Similar observations can be deduced from the quality factor results depicted in **Figure 3(f)**, as the Co amount is increased the quality factor decrease, suggesting weak coupling due to the decrease in surface to volume ratio.

Hence, we can seamlessly assume that the presence of Co is modifying the radiative bandwidth of Co-Ag nanoparticles and working under the assumptions highlighted above, it is safe to calculate the radiative bandwidth of Co-Ag by considering the whole nanoparticle equivalent to a single Ag nanoparticle of the same volume. This way the radiative quantum efficiency for the Ag and Co-Ag nanoparticles is calculated and plotted in **Figure 6(d)** as a function of plasmon resonance energy. So, by controlling the Co amount, the radiative quantum efficiency of Ag is tuned in a much wider energy range.

5. Other symbiotic systems

The above examples suggest that the synthesis of bimetallic or multi-metallic nanoparticles offers a wide variety of possibilities to tune/enhance or even discover new phenomenon occurring at the nanoscale. Symbiosis is not just limited to metals but is possible in other material systems as well. Few examples of widely studied combination of materials showing symbiosis are Au with Ag/Pd/Co or ZnO/SnO_2 systems. By synthesizing core-shell nanoparticles of Au-Ag, the optical properties of Au could be tuned below its inter-band transition [6]. The other interesting feature of core-shell nanoparticle is that by tuning the thickness of Ag shell, the bimetallic nanoparticle can sustain Fano resonance and Ag outer shell can provide chemical stability in harsh chloride ion environment due to the electron transfer from the Au core to the Ag shell [6, 44]. Au nanostructures also show a symbiotic relationship with Pd, by demonstrating better plasmonic refractive index sensing in Au-Pd core-shell nanoparticles over pure Au nanostructures [62]. On the other hand, the presence of plasmonic property of Au enhances the H_2 detection limit of Au-Pd bimetal system over pure Pd nanostructures [63]. In addition to looking at individual metal pairs, magneto-plasmonic (MP) field itself shows symbiosis at the nanoscale. The study of magneto-optics or active plasmonics is a mix of plasmonic and magnetic properties. Enhancement in magneto-optical (MO) activity occurs due to the presence of plasmonic resonance excitation causing electromagnetic field enhancement in the MO material. On the other hand, in active plasmonics, the plasmonic properties are tuned by the application of the external magnetic field. Co-Au system best describes the MP system, in which thin films of Co/Au tends to show active plasmonic while Au/Co/Au disks tend to show enhanced MO activity [4, 64]. Metal oxide system of ZnO/SnO_2 which forms a heterojunction also tends to show symbiosis at the nanoscale. Synthesizing core-shell nanowires of SnO_2-ZnO tends to demonstrate better NO_2 gas sensing under UV radiation over pure ZnO or SnO_2 nanowires [65]. The enhancement is due to the increased resistance caused by the photogeneration of electron-hole pairs under UV light. On the other hand, SnO_2 nanostructures stabilize ZnO in an aqueous environment, improves its biocompatibility and help tailor the excitonic luminescence properties [66].

6. Conclusions

In this chapter, we have provided a glimpse of the endless possible symbiotic properties observed at the nanoscale due to the interaction between nanomaterials demonstrating different properties. By selecting the right combination of materials, we demonstrated that their properties can be uniquely tailored as well as new characteristics can evolve. We highlight that there are a number of possible ways for material selection to synthesize multi-functional nanomaterials. The choice can be made per their position in the periodic table, their position in the chemical potential series, according to their properties or by their metallurgical interactions. The properties are not limited to the choice of material but can be tuned by controlling the shape, size and the dielectric environment of the nanomaterial. The research at the nanoscale has opened up a number of possibilities, which were not feasible a few decades ago. By controlling the nanoparticle morphology, Ni nanopillars have shown plasmon resonance in the visible spectrum of light while Au being diamagnetic has shown MO activity in pure Au nanodisks [55, 67]. These few discoveries point to the fact that nanotechnology is a vast pool of unknowns.

This book chapter focused on the symbiosis observed in bimetallic Co-Ag nanoparticles synthesized by PLiD. This was achieved by the synthesis route followed and the parameters considered while selecting the materials. Synthesis of bimetallic Co-Ag nanoparticles by PLiD helped in achieving segregated regions of Co and Ag within a single nanoparticle. This was confirmed by core-loss EELS mapping of the bimetallic nanoparticle. These nanoparticles were characterized for their optical properties by UV-vis spectroscopy and low-loss EELS. These bimetals showed improved or wider tuning of properties of their individual metal components which could be explained by the mutual sharing of free electrons between them, which had an uncanny resemblance to the symbiosis, observed in nature. The symbiotic properties can be broken down into two sections: (1) Co being the beneficiary and (2) Ag being the beneficiary. The examples for the former case can be summarized as the existence of a new surface plasmon resonance on Co surface, which was called as Ferroplasmon, whose discovery was facilitated by low-loss EELS study, and the enhancement in MO activity observed in these bimetallic Co-Ag nanoparticles (not discussed here) [22]. Similar observations for the latter case are the galvanic coupling, plasmon resonance tuning, enhancement in the plasmon quality factor and tuning of radiative quantum efficiencies. These few examples suggest the choice of materials and their properties can open new research fields which are not just limited to plasmonic and magnetic materials.

Acknowledgements

Ritesh Sachan acknowledges the National Academy of Sciences (NAS), USA, for awarding the NRC research fellowship. Ritesh Sachan also acknowledges ARO Grant No. W911NF-16-2-0038. Authors are also thankful for the useful discussions with John Prater and Ramki Kalyanaraman during the preparation of this chapter.

Author details

Abhinav Malasi[1]* and Ritesh Sachan[2,3]*

*Address all correspondence to: amalasi@utk.edu and rsachan@ncsu.edu

1 StudyFox, Leudelange, Luxembourg

2 Materials Science Division, Army Research Office, Research Triangle Park, North Carolina, USA

3 Department of Materials Science and Engineering, North Carolina State University, Raleigh, North Carolina, USA

References

[1] LaJeunesse TC, Thornhill DJ, Cox EF, Stanton FG, Fitt WK, Schmidt GW. High diversity and host specificity observed among symbiotic dinoflagellates in reef coral communities from Hawaii. Coral Reefs. 2004;**23**:596-603. DOI: 10.1007/s00338-004-0428-4

[2] Tilman D, Snell-Rood EC. Diversity breeds complementarity. Nature. 2014;**515**:44-45. DOI: 10.1038/nature13929

[3] Armelles G, Cebollada A, Garcia-Martin A, Gonzalez MU. Magnetoplasmonics: Combining magnetic and plasmonic functionalities. Advanced Optical Materials. 2013; **1**:10-35. DOI: 10.1002/adom.201200011

[4] Temnov VV, Armelles G, Woggon U, Guzatov D, Cebollada A, Garcia-Martin A, et al. Active magneto-plasmonics in hybrid metal-ferromagnet structures. Nature Photonics. 2010;**4**:107-111. DOI: 10.1038/nphoton.2009.265

[5] Linic S, Christopher P, Ingram DB. Plasmonic-metal nanostructures for efficient conversion of solar to chemical energy. Nature Materials. 2011;**10**:911-921. DOI: 10.1038/nmat3151

[6] Pena-Rodriguez O, Pal U. Au@Ag core-shell nanoparticles: Efficient all-plasmonic Fano-resonance generators. Nanoscale. 2011;**3**:3609. DOI: 10.1039/C1NR10625B

[7] Guo S, Dong S, Wang E. Three-dimensional Pt-on-Pd bimetallic nanodendrites supported on graphene nanosheet: Facile synthesis and used as an advanced nanoelectrocatalyst for methanol oxidation. ACS Nano. 2010;**4**:547-555. DOI: 10.1021/nn9014483

[8] Favazza C, Kalyanaraman R, Sureshkumar R. Robust nanopatterning by laser-induced dewetting of metal nanofilms. Nanotechnology. 2006;**17**:4229-4234. DOI: 10.1088/0957-4484/17/16/038

[9] Trice J, Thomas D, Favazza C, Sureshkumar R, Kalyanaraman R. Pulsed-laser-induced dewetting in nanoscopic metal films: Theory and experiments. Physical Review B. 2007;**75**:235439. DOI: 10.1103/PhysRevB.75.235439

[10] Sharma A, Jameel AT. Nonlinear stability, rupture and morphological phase separation in thin fluids on apolar and polar substrates. Journal of Colloid and Interface Science. 1993;**161**:190-208. DOI: 10.1006/jcis.1993.1458

[11] Krishna H, Shirato N, Yadavali S, Sachan R, Strader J, Kalyanaraman R. Self-organization of nanoscale multilayer liquid metal films: Experiment and theory. ACS Nano. 2011;**5**:470-476. DOI: 10.1021/nn1022632

[12] Sachan R, Yadavali S, Shirato N, Krishna H, Ramos V, Duscher G, et al. Self-organized bimetallic Ag-Co nanoparticles with tunable localized surface plasmons showing high environmental stability and sensitivity. Nanotechnology. 2012;**23**:275604 (1-8). DOI: 10.1088/0957-4484/23/27/275604

[13] Malasi A, Taz H, Ehrsam M, Goodwin J, Garcia H, Kalyanaraman R. Enhanced and tunable optical quantum efficiencies from plasmon bandwidth engineering in bimetallic CoAg nanoparticles. APL Photonics. 2016;**1**:76101. DOI: 10.1063/1.4954698

[14] Yadavali S, Kalaynaraman R. Nanomaterials synthesis by a novel phenomenon: The nanoscale Rayleigh-Taylor instability. AIP Advances. 2014;**4**:47116. DOI: 10.1063/1.4871482

[15] Hulteen JC, Van Duyne RP. Nanosphere lithography: A materials general fabrication process for periodic particle array surfaces. Journal of Vacuum Science and Technology A. 1995;**13**:1553-1558. DOI: 10.1116/1.579726

[16] Meng X, Qiu D. Gas-flow-induced reorientation to centimeter-sized two-dimensional colloidal single crystal of polystyrene particle. Langmuir. 2014;**30**:3019-3023. DOI: 10.1021/la404944w

[17] Jensen TR, Schatz GC, Van Duyne RP. Nanosphere lithography: Surface plasmon resonance spectrum of a periodic array of silver nanoparticles by ultraviolet-visible extinction spectroscopy and electrodynamic modeling. The Journal of Physical Chemistry B. 1999;**103**:2394-2401. DOI: 10.1021/jp984406y

[18] Denkov ND, Velev OD, Kralchevsky PA, Ivanov IB, Yoshimura H, Nagayama K. Two-dimensional crystallization. Nature. 1993;**361**:26. DOI: 10.1038/361026a0

[19] Rakers S, Chi LF, Fuchs H. Influence of the evaporation rate on the packing order of polydisper latex monofilms. Langmuir. 1997;**13**:7121-7124. DOI: 10.1021/la970757c

[20] Amos RM, Rarity JG, Tapster PR, Shepherd TJ, Kitson SC. Fabrication of large-area face-centered-cubic hard-sphere colloidal crystals by shear alignment. Physical Review E. 2000;**61**:2929. DOI: 10.1103/PhysRevE.61.2929

[21] Kuai SL, Hu XF, Hache A, Truong VV. High-quality colloidal photonic crystals obtained by optimizing growth parameters in a vertical deposition technique. Journal of Crystal Growth. 2004;**267**:317-324. DOI: 10.1016/j.jcrysgro.2004.03.015

[22] Malasi A. Symbiotic plasmonic nanomaterials: Synthesis and properties [thesis]. Knoxville: University of Tennessee; 2016

[23] Malasi A, Ge J, Carr C, Garcia H, Duscher G, Kalyanaraman R. Two-dimensionally ordered plasmonic and magnetic nanostructures on transferable electron transparent

substrates. Particle and Particle Systems Characterization. 2015;**32**:970-978. DOI: 10.1002/ppsc.201500048

[24] Nemiroski A, Gonidec M, Fox JM, Jean-Remy P, Turnage E, Whitesides GM. Engineering shadows to fabricate optical metasurfaces. ACS Nano. 2014;**8**:11061-11070. DOI: 10.1021/nn504214b

[25] Fredriksson H, Alaverdyan Y, Dmitriev A, Langhammer C, Sutherland DS, Zach M, et al. Hole-mask colloidal lithography. Advanced Materials. 2007;**19**:4297-4302. DOI: 10.1002/adma.200700680

[26] Kosiorek A, Kandulski W, Glaczynska H, Giersig M. Fabrication of nanoscale rings, dots, and rods by combining shadow nanosphere lithography and annealed polystyrene nanosphere masks. Small. 2005;**1**:439-444. DOI: 10.1002/smll.200400099

[27] Haynes CL, McFarland AD, Smith MT, Hulteen JC, Van Duyne RP. Angle-resolved nanosphere lithography: Manipulation of nanoparticle size, shape, and interparticle spacing. The Journal of Physical Chemistry B. 2002;**106**:1898-1902. DOI: 10.1021/jp013570+

[28] Schneider CA, Rasband WS, Eliceiri KW. NIH Image to ImageJ: 25 years of image analysis. Nature Methods. 2012;**9**:671-675. DOI: 10.1038/nmeth.2089

[29] Sachan R, Ramos V, Malasi A, Yadavali S, Bartley B, Garcia H, et al. Oxidation-resistant silver nanostructures for ultrastable plasmonic applications. Advanced Materials. 2013; **25**:2045-2050. DOI: 10.1002/adma.201204920

[30] Gilroy KD, Ruditskiy A, Peng H-C, Qin D, Xia Y. Bimetallic nanocrystals: Syntheses, properties, and applications. Chemical Reviews. 2016;**116**:10414-10472. DOI: 10.1021/acs.chemrev.6b00211

[31] Mayer KM, Hafner JH. Localized surface plasmon resonance sensors. Chemical Reviews. 2011;**111**:3828-3857. DOI: 10.1021/cr100313v

[32] Sachan R, Malasi A, Ge J, Yadavali S, Krishna H, Gangopadhyay A, et al. Ferroplasmons: Intense localized surface plasmons in metal-ferromagnetic nanoparticles. ACS Nano. 2014;**8**:9790-9798. DOI: 10.1021/nn5031719

[33] Khenner M, Yadavali S, Kalyanaraman R. Controlling nanoparticles formation in molten metallic bilayers by pulsed-laser interference heating. Mathematical Modelling of Natural Phenomena. 2012;**7**:20-38. DOI: 10.1051/mmnp/20127403

[34] Malasi A, Sachan R, Ramos V, Garcia H, Duscher G, Kalaynaraman R. Localized surface plasmon sensing based investigation of nanoscale metal oxidation kinetics. Nanotechnology. 2015;**26**:205701. DOI: 10.1088/0957-4484/26/20/205701

[35] Sachan R, Malasi A, Yadavali S, Griffey B, Dunlap J, Duscher G, et al. Laser induced self-assembled nanostructures on electron transparent substrates. Particle and Particle Systems Characterization. 2015;**32**:476-482. DOI: 10.1002/ppsc.201400183

[36] Garcia H, Kalyanaraman R, Sureshkumar R. Nonlinear optical properties of multi-metal nanocomposites in a glass matrix. Journal of Physics B: Atomic, Molecular and Optical Physics. 2009;**42**:175401. DOI: 10.1088/0953-4075/42/17/175401

[37] Link S, El-Sayed MA. Shape and size dependence of radiative, non-radiative and photothermal properties of gold nanocrystals. International Reviews in Physical Chemistry. 2000;**19**:409-453. DOI: 10.1080/01442350050034180

[38] Link S, El-Sayed MA. Spectral properties and relaxation dynamics of surface plasmon electronic oscillations in gold and silver nanodots and nanorods. The Journal of Physical Chemistry B. 1999;**103**:8410-8426. DOI: 10.1021/jp9917648

[39] West PR, Ishii S, Naik GV, Emani NK, Shalaev VM, Boltasseva A. Searching for better plasmonic materials. Laser & Photonics Reviews. 2010;**4**:795-808. DOI: 10.1002/lpor.200900055

[40] Han Y, Lupitskyy R, Chou T-M, Stafford CM, Du H, Sukhishvili S. Effect of oxidation on surface-enhanced Raman scattering activity of silver nanoparticles: A quantitative correlation. Analytical Chemistry. 2011;**83**:5873-5880. DOI: 10.1021/ac2005839

[41] Losurdo M, Bergmair I, Giangregorio MM, Dastmalchi B, Bianco GV, Helgert C, et al. Enhancing chemical and optical stability of silver nanostructures by low-temperature hydrogen atoms processing. The Journal of Physical Chemistry C. 2012;**115**:23004-23012. DOI: 10.1021/jp307936k

[42] Naik GV, Kim J, Boltasseva A. Oxides and nitrides as alternative plasmonic materials in the optical range. Optical Materials Express. 2011;**1**:1090-1099. DOI: 10.1364/OME.1.001090

[43] Naik GV, Shalaev VM, Boltasseva A. Alternative plasmonic materials: Beyond gold and silver. Advanced Materials. 2013;**25**:3264-3294. DOI: 10.1002/adma.201205076

[44] Shankar C, Dao ATN, Singh P, Higashimine K, Mott DM, Maenosono S. Chemical stabilization of gold coated by silver core-shell nanoparticles via electron transfer. Nanotechnology. 2012;**23**:1-10. DOI: 10.1088/0957-4484/23/24/245704

[45] Li X, Li J, Zhou X, Ma Y, Zheng Z, Duan X, et al. Silver nanoparticles protected by monolayer graphene as a stabilized substrate for surface enhanced Raman spectroscopy. Carbon. 2014;**66**:713-719. DOI: 10.1016/j.carbon.2013.09.076

[46] Fafarman AT, Hong SH, Oh SJ, Caglayan H, Ye X, Diroll BT, et al. Air-stable, nanostructured electronic and plasmonic materials from solution-processable, silver nanocrystal building block. ACS Nano. 2014;**8**:2746-2754. DOI: 10.1021/nn406461p

[47] Garcia H, Sachan R, Kalyanaraman R. Optical plasmon properties of Co-Ag nanocomposites within the mean-field approximation. Plasmonics. 2012;**7**:137-141. DOI: 10.1007/s11468-011-9286-4

[48] Malasi A, Kalyanaraman R, Garcia H. From Mie to Fresnel through effective medium approximation with multipole contributions. Journal of Optics. 2014;**16**:65001. DOI: 10.1088/2040-8978/16/6/065001

[49] Farah AE, Davidson R, Malasi A, Pooser RC, Lawrie B, Kalyanaraman R. Cobalt stabilization of silver extraordinary optical transmission sensing platforms. Applied Physics Letters. 2016;**108**:43101. DOI: 10.1063/1.4940389

[50] Prodan E, Radloff C, Halas NJ, Nordlander P. A hybridization model for the plasmon response of complex nanostructures. Science. 2003;**302**:419-422. DOI: 10.1126/science.1089171

[51] Miroshnichenko AE, Flach S, Kivshar YS. Fano resonances in nanoscale structures. Reviews of Modern Physics. 2010;**82**:2257-2298. DOI: 10.1103/RevModPhys.82.2257

[52] Mukherjee S, Sobhani H, Lassiter JB, Bardhan R, Nordlander P, Halas NJ. Fanoshells: Nanoparticles with built-in Fano resonances. Nano Letters. 2010;**10**:2694-2701. DOI: 10.1021/nl1016392

[53] Cetin AE, Altug H. Fano resonant ring/disk plasmonic nanocavities on conducting substrates for advanced biosensing. ACS Nano. 2012;**6**:9989-9995. DOI: 10.1021/nn303643w

[54] Chen F, Alemu N, Johnston RL. Collective plasmon modes in a compositionally asymmetric nanoparticle dimer. AIP Advances. 2011;**1**:032134 (1-16). DOI: 10.1063/1.3628346

[55] Chen J, Albella P, Pirzadeh Z, Alonso-Gonzalez P, Huth F, Bonetti S, et al. Plasmonic nickel nanoantennas. Small. 2011;**7**:2341-2347. DOI: 10.1002/smll.201100640

[56] Ge J, Malasi A, Passarelli N, Pérez LA, Coronado EA, Sachan R, et al. Ferroplasmons: Novel plasmons in metal-ferromagnetic bimetallic nanostructures. Microscopy and Microanalysis. 2015;**21**(S3):2381-2382. DOI: 10.1017/S1431927615012684

[57] Brongersma ML, Hartman JW, Atwater HA. Electromagnetic energy transfer and switching in nanoparticle chain arrays below the diffraction limit. Physical Review B. 2000;**62**:R16356-R16359. DOI: 10.1103/PhysRevB.62.R16356

[58] Passarelli N, Pérez LA, Coronado EA. Plasmonic interactions: From molecular plasmonics and Fano resonances to ferroplasmons. ACS Nano. 2014;**8**:9723-9728. DOI: 10.1021/nn505145v

[59] Sonnichsen C, Franzl T, Wilk T, von Plessen G, Feldmann J, Wilson O, et al. Drastic reduction of plasmon damping in gold nanorods. Physical Review Letters. 2002;**88**:77402. DOI: 10.1103/PhysRevLett.88.077402

[60] Wokaun A, Gordon JP, Liao PF. Radiation damping in surface-enhanced Raman-scattering. Physical Review Letters. 1982;**48**:957-960. DOI: 10.1103/PhysRevLett.48.957

[61] Tsakmakidis KL, Wartak MS, Cook JJH, Hamm JM, Hess O. Negative-permeability electromagnetically induced transparent and magnetically active metamaterials. Physical Review B. 2010;**81**:195128. DOI: 10.1103/PhysRevB.81.195128

[62] Sugawa K, Tahara H, Yamashita A, Otsuki J, Sagara T, Harumoto T, et al. Refractive index susceptibility of the plasmonic palladium nanoparticle: Potential as the third plasmonic sensing material. ACS Nano. 2015;**9**:1895-1904. DOI: 10.1021/nn506800a

[63] Jiang R, Qin F, Ruan Q, Wang J, Jin C. Ultrasensitive plasmonic response of bimetallic Au/Pd nanostructures to hydrogen. Advanced Functional Materials. 2014;**24**:7328-7337. DOI: 10.1002/adfm.201402091

[64] Meneses-Rodriguez D, Ferreiro-Vila E, Prieto P, Anguita J, Gonzalez MU, Garcia-Martin JM, et al. Probing the electromagnetic field distribution within a metallic nanodisk. Small. 2011;**7**(23):3317. DOI: 10.1002/smll.201101060

[65] Park S, An S, Mun Y, Lee C. UV-enhanced NO_2 gas sensing properties of SnO_2-core/ZnO-shell nanowires at room temperature. ACS Applied Materials & Interfaces. 2013;**5**:4285-4292. DOI: 10.1021/am400500a

[66] Roge V, Georgantzopoulou A, Mehennaoui K, Fechete I, Garin F, Dinia A, et al. Tailoring the optical properties of ZnO nano-layers and their effect on in vitro biocompatibility. RSC Advances. 2015;**5**:97635-97647. DOI: 10.1039/C5RA16156H

[67] Sepúlveda B, González-Díaz JB, García-Martín A, Lechuga LM, Armelles G. Plasmon-induced magneto-optical activity in nanosized gold disks. Physical Review Letters. 2010;**104**:147401. DOI: 10.1103/PhysRevLett.104.147401

IntechOpen